Dynamics and Control of a Reconfigurable Multi-Arm Robot for In-Orbit Assembly

Hrishik Mishra [*,**] **Marco De Stefano** [*] **Christian Ott** [**]

Institute of Robotics and Mechatronics, German Aerospace Center (DLR), 82234, Weßling, Germany. (e-mail: hrishik.mishra@dlr.de).
**Automation and Control Institute (ACIN), Technical University of Vienna, 1040 Vienna, Austria.*

Abstract - In this paper, a passivity-based controller is proposed for a reconfigurable multi-arm system, which is employed for in-orbit assembly. The reconfigurable system is composed of multiple anthropomorphic arms which can be connected to a torso or operate independently. The proposed control is applicable for all the morphologies of the multi-arm system while performing several operations required for the assembly task, such as walking on a telescope structure through dedicated mechanical interfaces. The constrained dynamics is exploited to derive a unified joint actuation control law for all the considered operations and morphologies. A Co-simulation framework was developed to simulate the operations for control prototyping, and simulation results prove the effectiveness of the proposed unified controller.

Keywords: Motion Control - Robots manipulators - Passivity-based control.

1. INTRODUCTION

Autonomous assembly of structures in orbit is a key technology for increasing the size of large structure in space. This technology is especially required for structures which are too large to be self-deployed as a single component. An example is the new generation of space telescopes, which requires a larger diameter for advance operations (see Deremetz et al. (2020)). However, the maximum possible size is limited mainly by the dimension of the launch vehicle (Roa et al. (2017)). A suitable solution is to deliver the components of the structure into the orbit in single or multiple launches and perform the so-called in-orbit assembly. Besides telescope assembly, other applications of in-space assembly include solar arrays for power plants, space transportation hub, in-situ resource utilization for construction and sun shields assembly (Belvin et al. (2016)).

Robotics emerges as a promising technology to perform the assembly tasks in orbit and it has been analysed in recent space mission studies, see e.g. the RAMST (Lee et al. (2016)), PULSAR (Roa et al. (2019)) or MOSAR (Deremetz et al. (2020)) projects. In these studies the robot is composed of one or multiple manipulator arms and it is used to climb or walk on top of the spacecraft carrying a module (e.g. a mirror tile of the telescope) to be assembled with the main structure in orbit. In this case the robot locomotion is enabled via the mechanical connection between the manipulator end-effector and the interface located on the mirror tile itself. These interfaces are namely called Standard Interface (SI) and they provide transferring of electrical signals and data. Examples of SIs are the SIROM and HOTDOCK interface (see Letier et al. (2020)). The motion of the robot through the SIs increases its workspace, which is not restricted to the reachability of the arm, but can be extended through the multiple attachment points on the SIs.

In an on-going ESA-funded project, MIRROR, a novel design of a modular Multi Arms Robot system (MAR) has
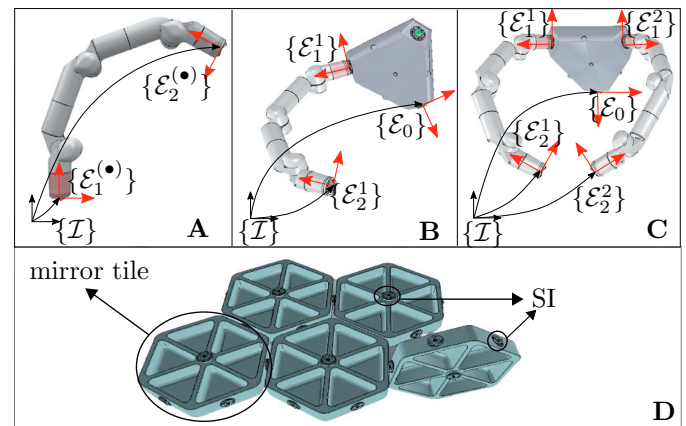

Figure 1. Morphologies of the MAR system in MIRROR project. **A**: Morphology 1-arm, **B**: Morphology 1-arm+torso, **C**: Morphology 2-arms, **D**: Breadboard of mirror tiles equipped with standard interfaces (SI).

been proposed (see (Deremetz et al. (2021))). The MAR is composed of three modules, a torso and two symmetrical 7-degrees of freedom (DOF) anthropomorphic arms that are functionally independent and can be connected through the SIs to the torso. The modular design approach of the MAR reduces the complexity of the robotic system by splitting it into a smaller number of components and taking advantage of separating and recombining the manipulators in different morphologies. Examples of the MAR morphology are: 1-arm, 1-arm+torso and 2-arms, which are shown in Fig. 1 **A**, **B** and **C**, respectively. The main operations foreseen for the MAR are pick and place of the tiles (shown in Fig. 1-**D**) with the torso or the arm(s) and walking or transportation of the tiles on the telescope structure through the SIs. These operations will allow to extend the dimension of the telescope structure in orbit.

While the kinematics of the two-arms orbital MAR system at the first glance resembles a terrestrial bipedal robot, its dynamics has some important differences. Research

★ H. Mishra and M. De Stefano contributed equally to this work.

on terrestrial locomotion with bipedal and multi-legged robots is concerned with the unstable dynamics of the robot's center of mass under the effect of gravity. Motion generation and gait stabilization have profited strongly from simplified models such as the inverted pendulum model, as shown in Kajita (2019). In legged robots the center of mass is propelled forward by the contact forces between the feet and the ground so that the range of possible motions is restricted by the unilateral contact constraints. Often these unilateral constraints are handled in the motion generation and control algorithms in a more intuitive way by the use of ground reference points such as the zero moment point, the centroidal moment pivot, or the center of pressure (see Vukobratovic and Borovac (2004); Popovic et al. (2005)).

The orbital locomotion problem for the MAR system differs in several ways from terrestrial locomotion. Most importantly, the absence of gravity simplifies the gait stabilization problem and allows to decouple the geometric path planning from the contact stabilization. Secondly, the contacts established by the docking interfaces, namely the SIs located at the end-effectors and the torso, can be modelled as bilateral holonomic constraints. In contrast to the unilateral constraints appearing in legged locomotion, which are typically modelled by means of complementarity problems, these bilateral contact constraints can be modelled as holonomic constraints limited by a maximal allowed contact force. Finally, the MAR system applies various contact transitions at the three standard interfaces. As a consequence, several multi-contact cases have to be handled for the MAR system, with one or two links in contact with the environment. For terrestrial legged locomotion, the force distribution problem during double stance as well as in more complex multi-contact conditions has successfully been handled by the passivity based balancing controller in (Henze et al. (2016)). Therein, an optimization problem for the control forces is solved at each time instance taking the unilateral contact force constraints into account. In contrast to an inverse dynamics based formulation as used e.g. in (Righetti et al. (2013)), the controller from Henze et al. (2016) is aiming at a desired compliance for the center of mass and the free end-effectors. This leads to a closed loop dynamics in which the natural inertia is preserved, which has benefits for the robustness, as shown in Dietrich et al. (2021).

1. Problem Statement and Contribution: In contrast to common modelling and methods for terrestrial locomotion discussed above, the MAR system is subjected to bilateral constraints established via the latching of the SIs and it operates in absence of gravity. A unique aspect of the MAR is its modular design, which requires operations in different morphologies (see Fig. 1). This requires the handling of multi-contacts for preforming several operations, which are listed as follows:

　A Morphology 1-arm:
　　(i) walking operation on the SIs of the mirror tiles
　　(ii) pick and place of the tile
　B Morphology 1-arm+torso:
　　(i) walking operation on the SIs of the mirror tiles
　　(ii) pick and place of the tile
　C Morphology 2-arms:
　　(i) walking operation of the mirror tiles
　　(ii) torso operation, i.e. control the torso while the 2-arms are connected to the SIs
　　(iii) dual-arm operation, i.e. controlling the arms while the torso is connected to a SI.

Considering the three morphologies defined above and the multiple operations which the MAR needs to handle, a unified control design is required to address all the operations in a stable manner. Although a common approach is to reduce the floating-base dynamics to a smaller set of unconstrained equations for a specific task (see De Sapio (2011)), the multiplicity of morphologies and operations poses a challenge for a unified design. This factor defines the scope of this paper.

The contribution of this paper is twofold. Firstly, a unified passivity-based Cartesian impedance controller is designed in order to accommodate all the MAR operations for each morphology listed above (1-arm, 1-arm+torso and 2-arms) and shown in Fig. 1. To this end, we use the constrained dynamics in the analysis to derive a unified joint actuation control law, which is compliant against the constraint forces. A key advantage of the proposed controller is that it can operate in both decentralized and centralized manner. Secondly, a Co-simulation framework is developed for control prototyping and used for the validation of the MAR operations, and its results are presented.

The structure of the paper is defined as follows. Sec. 2 introduces the modelling of the MAR system, Sec. 3 shows the designed control, which can operate for all the morphologies and Sec. 4 introduces the Co-simulation framework developed for the validation. Validation results are shown in Sec. 5 with concluding remarks in Sec. 6.

2. UNIFIED MODELLING: FLOATING-BASE DYNAMICS

In this section, the modelling of the MAR system is performed. Its current morphology is denoted as $x \in \mathcal{S}$, where $\mathcal{S} = \{\mathbf{A}, \mathbf{B}, \mathbf{C}\}$ is the set of all morphologies labelled in Fig. 1. The complete configuration of each morphology in Fig. 1 is $r = (g_b, q) \in \mathrm{SE}(3) \times \mathbb{R}^n$, where $g_b \in \mathrm{SE}(3)$ is the pose of a body-fixed frame, $\{B\}$, and $q \in \mathbb{R}^n$ is the vector of revolute joint positions. Note that the body-fixed frame is $\{\mathcal{B}\} = \{\mathcal{E}_1^{(\bullet)}\}$ for the 1-arm case, and $\{\mathcal{B}\} = \{\mathcal{E}_0\}$ for the latter two cases in Fig. 1. Additionally, considering N_a as the maximal number of arms in the $\mathbf{C}$ morphology of Fig. 1, each with n_a number of joints, we obtain $n = n_a$, for $\mathbf{A}, \mathbf{B}$ and $n = N_a.n_a$ for $\mathbf{C}$, respectively. In particular, for the MIRROR case, $n_a = 7$ and $N_a = 2$.

The SE(3) differential kinematics are $\dot{g}_b = g_b V_b^\wedge$, where $V_b \in \mathbb{R}^6$ is the body velocity and $(\bullet)^\wedge : \mathbb{R}^6 \mapsto \mathfrak{se}(3)$ is the isomorphism (Bullo and Murray (1999)). Using the configuration velocities, $V = \begin{bmatrix} V_b^\top & \dot{q}^\top \end{bmatrix}^\top$, the motion of the MAR system is given by the system of Hamel equations (Saccon et al. (2017)), as ,

$$M(q) \begin{bmatrix} \dot{V}_b \\ \ddot{q} \end{bmatrix} + C(q, V_b, \dot{q}) \begin{bmatrix} V_b \\ \dot{q} \end{bmatrix} = \begin{bmatrix} 0_6 \\ \tau \end{bmatrix} \qquad (1)$$

where $M = \begin{bmatrix} M_b & M_{bq} \\ M_{bq}^\top & M_q \end{bmatrix}$ is the coupled inertia matrix, with M_b, M_{bq}, M_q as the locked, coupling and joint inertia sub-matrices respectively. Additionally, C is non-unique matrix of Coriolis and centrifugal terms, and $\tau \in \mathbb{R}^n$ is covector of joint actuation.

To generalize the control design in the following section, $g_j^k \in \mathrm{SE}(3)$ with $j = [1, 2]$ and $k = [1, ..N_a]$, is the pose of the jth end-effector on the kth arm with respect to the inertial frame $\{\mathcal{I}\}$. Similarly, $V_j^k \in \mathbb{R}^6$, is the body velocity of the corresponding frame, and g_0, V_0 are the pose and body velocity of the torso with respect to inertial frame, $\{\mathcal{I}\}$. The superscript k will denote the arm label, and the subscript j will indicate the end-effector label.

The SIs on the tiles are assumed to be inertially fixed. When the MAR system is attached to the SIs, it is holonomically constrained. Specifically, these constraints are defined as,

$$\{g_1^{(\bullet)} = const, V_1^{(\bullet)} = 0_6\} \tag{2a}$$

$$\{g_2^{(\bullet)} = const, V_2^{(\bullet)} = 0_6\} \tag{2b}$$

$$\{g_0 = const, V_0 = 0_6\} \tag{2c}$$

The constraints (2a)-(2c) can be written separately or in any combination as,

$$\underbrace{[\Psi_b(q)\ \Psi_q(q)]}_{\Psi(q)} \begin{bmatrix} V_b \\ \dot{q} \end{bmatrix} = 0 \Rightarrow V_b = -\underbrace{\Psi_b^\dagger \Psi_q}_{\Psi_{bq}} \dot{q} \tag{3}$$

where Ψ is the constraint Jacobian, and $(\bullet)^\dagger$ is the pseudo-inverse of the argument. In this paper, we consider operations with more than 1 constraint. Hence, Ψ_b is full column rank and the solution on R.H.S of (3) is unique.

Due to these constraints, (1) is modified as,

$$M(q) \begin{bmatrix} \dot{V}_b \\ \ddot{q} \end{bmatrix} + C(q, \dot{q}, V_b) \begin{bmatrix} V_b \\ \dot{q} \end{bmatrix} + \Psi(q)^\top \lambda = \begin{bmatrix} 0_6 \\ \tau \end{bmatrix} \tag{4}$$

where λ is the vector of Lagrangian multipliers (constraint forces). The model in (4) possesses the following property, which will be used for the stability analysis.

Property 1. The inertia matrix, $M \succ 0$, is positive definite and satisfies the skew-symmetric property, i.e., $V^\top(\dot{M} - 2C)V = 0$.

3. UNIFIED CONTROL DESIGN

This section proposes the design of a unified passivity-based controller which can operate in all the morphologies of the MAR system shown in Fig. 1, denoted with state variable $x = [\mathbf{A}, \mathbf{B}, \mathbf{C}]$. To accommodate the control tasks required in different morphologies and operations, we exploit the constrained dynamics to compute a unified joint actuation control law.

To achieve the desired operational tasks, the desired set-point(s) is(are) given by the pose(s) of the Cartesian frame(s) of the SI located on a mirror tile (see Fig. 1-**D**). In particular, a setpoint is defined as $g^* \in \mathcal{D} \subset \text{SE}(3)^l$, where $\mathcal{D}$ is a set that contains l tiles in the reachable neighbourhood of the MAR system. For the morphology $x = \mathbf{A}$ in Fig. 1, the setpoint(s) for walking are defined for either $\mathcal{E}_1^{(\bullet)}$ or $\mathcal{E}_2^{(\bullet)}$. For $x = \mathbf{B}$, the setpoint(s) for the same operation are defined for $\mathcal{E}_1^{(\bullet)}$ or $\mathcal{E}_0$. For $x = \mathbf{C}$, the setpoint(s) for walking are defined for $\mathcal{E}_2^1$ or $\mathcal{E}_2^2$, for torso control as $\mathcal{E}_0$, and arm-control as $\mathcal{E}_2^1$ and $\mathcal{E}_2^2$.

The following lemmas are introduced in order to define the potential functions and configuration velocity, which will be later exploited to prove the stability of the controller.

Lemma 1. Given a task pose $g(R, p) \in \text{SE}(3)$ and a desired setpoint $g_d(R_d, p_d) \in \text{SE}(3)$, the task error is defined as $\eta = g_d^{-1} g \equiv (\check{\eta}, r) = (R_d^\top R, R^\top(p - p_d))$. The task is formally described by the positive SE(3) potential energy, $\Phi(K, \mathcal{K}, \eta) = \phi(K, \check{\eta}) + \frac{1}{2}\|r\|_\mathcal{K}^2$, where $K, \mathcal{K} \in \mathbb{R}^{3\times3}$ are respectively the rotational and translational proportional gain matrix and $\phi = \frac{1}{2}\text{tr}(K(\mathbb{I}_{3,3} - \check{\eta}))$ is the SO(3) potential. The positive-definiteness of Φ is ensured by, firstly, $\mathcal{K} \succ 0$, and, secondly, $K = \text{blkdiag}(k_1, k_2, k_3)$ with $k_i > 0$. The potential is bounded as $\underline{\Phi} < \Phi < \overline{\Phi}$ due to the bounded-ness of translational and rotational parts, as shown in

Mishra et al. (2020). At equilibrium, i.e., $\eta = \mathbb{I}_{4,4}$, $\Phi = 0$. The time-derivative of Φ is obtained, as in (Mishra et al., 2020, eq. (22)), as,

$$\dot{\Phi} = \gamma(\eta)^\top V, \quad \gamma = \begin{bmatrix} \zeta(K, \check{\eta}) \\ \check{\eta}^\top \mathcal{K} r \end{bmatrix}, \tag{5}$$

where $\gamma \in \mathbb{R}^6 \cong \mathfrak{se}(3)^*$ is the proportional wrench for the potential, Φ, $\zeta = [\text{sk}(K\check{\eta})]^\vee$ and $\text{sk}(\bullet)$ is the skew-symmetric part of the argument, and $(\bullet)^\vee : \mathfrak{so}(3) \mapsto \mathbb{R}^3$ (Bullo and Murray (1999)).

The choice of η, Φ in *Lemma 1* ensures that the proportional gains, $K, \mathcal{K}$, are in the desired frame, which provides an intuitive way to set the desired stiffness.

Note that each of the N_a arms has two end-effectors, $\{\mathcal{E}_1^{(\bullet)}\}$ and $\{\mathcal{E}_2^{(\bullet)}\}$, in Fig. 1. Reconfigurability of the arm refers to the ability to use any one of these end-effectors to perform attachment with either SI or torso. Therefore, to accommodate a unified approach for controlling all the end-effectors and also the torso, the potential function is taken as the sum of $2N_a + 1$ potentials.

Def. 1. Generalized Virtual Potential Function: For any morphology, x, as described in Fig. 1, the operations in Sec. 1-1 are accommodated using a common potential as,

$$\hat{\Phi}(\eta_0, \eta_1^1, \eta_2^1...\eta_1^{N_a}, \eta_2^{N_a}) = \Phi(\eta_0) + \sum_{k=1}^{N_a} \sum_{j=1}^{2} s_j^k \Phi(\eta_j^k) \tag{6}$$

where Φ is used from *Lemma 1*, $\eta_0 = g_{0d}^{-1} g_0$ and $\eta_j^k = g_{jd}^{k^{-1}} g_j^k$ with g_{0d}, g_{jd}^k are the corresponding setpoints, and $s_j^k = [0, 1]$ is a selector value such that $s_j^k = 0$, if the jth end-effector of the kth arm is attached to the torso, and $s_j^k = 1$, otherwise. In the following stability analysis, s_j^k remains constant throughout an atomic operation.

Lemma 2. For the MAR system in any morphology, x, as in Fig. 1, the body velocity of an end-effector-fixed frame, $\{\mathcal{E}_j^k\}$, where $k = [p|p \in \mathbb{N}, p \leq N_a]$ and $j = [1, 2]$, is written in terms of configuration velocity, V, as

$$V_j^k = T_{bj}^k V_b + T_{qj}^k \dot{q} \tag{7}$$

where $T_{bj}^k = g_j^{k^{-1}} \frac{\partial g_j^k}{\partial g_b} \in \mathbb{R}^{6\times6}$ is the base Jacobian and $T_{qj}^k = g_j^{k^{-1}} \frac{\partial g_j^k}{\partial q} \in \mathbb{R}^{6\times n}$ is the manipulator Jacobian.

The unified control law is given by the following.

Theorem 1. For the MAR system in any morphology, x, as described in Fig. 1, and all the operations defined in Sec. 1-1, the control law for the joint actuation given by

$$\tau = \Psi_{bq}^\top \underbrace{(\gamma_0 + D_0 V_b)}_{\text{PD}_0} - \sum_{k=1}^{N_a} \sum_{j=1}^{2} s_j^k \tilde{T}_{qj}^{k^\top} \underbrace{(\gamma_j^k + D_{jk} V_j^k)}_{\text{PD}_j^k}$$
$$\underbrace{-(N_0^\top P_0 N_0 + \sum_{k=1}^{N_a} \sum_{j=1}^{2} N_j^{k^\top} P_{jk} N_j^k)\dot{q}}_{\tau_n} \tag{8}$$

ensures the uniform asymptotic stability of the states, i.e., $\eta_0, \eta_{1k}, \eta_{2k} \to \mathbb{I}_{4,4}$ and $V_{1k}, V_{2k}, V_0 \to 0_6$, where Ψ_{bq} is the constraint matrix from the R.H.S. equality of (3), $\tilde{T}_{qj}^k = T_{qj}^k - T_{bj}^k \Psi_{bq}$ is the constraint reduced task Jacobian, and $N_0 = (\mathbb{I}_{n,n} - \Psi_{bq}^\top \Psi_{bq}^{\dagger^\top})$, $N_j^k = (\mathbb{I}_{n,n} - \tilde{T}_{qj}^{k^\top} \tilde{T}_{qj}^{k\dagger^\top})$ are the null-space projections and $D_0, D_j^k, P_0, P_{jk} \succ 0$.

Proof. Lyapunov's direct method is used to prove convergence, and the candidate function is chosen as the sum of the MAR kinetic energy and the generalized virtual potential function from *Def. 1* as,

$$W = \frac{1}{2}\langle V, V \rangle_{M(q)} + \hat{\Phi}(\eta_0, \eta_1^1, \eta_2^1 ... \eta_1^{N_a}, \eta_2^{N_a}) \quad (9)$$

where $V = \begin{bmatrix} V_b^\top & \dot{q}^\top \end{bmatrix}^\top$. Using the property 1, taking the time-derivative of (9), we obtain,

$$\dot{W} = V^\top \begin{bmatrix} 0_6 + \Psi_b^\top \lambda \\ \tau + \Psi_q^\top \lambda \end{bmatrix} + \gamma_0^\top V_0 + \sum_{k=1}^{N_a} \sum_{j=1}^{2} s_j^k \gamma_j^{k^\top} V_j^k \quad (10)$$

Using *Lemma 2*, V_j^k is expanded to rewrite (10) as,

$$\dot{W} = V^\top \begin{bmatrix} \Psi_b^\top \lambda + \gamma_0 + \sum_{k=1}^{N_a} \sum_{j=1}^{2} s_j^k T_{bj}^{k^\top} \gamma_j^k \\ \tau + \Psi_q^\top \lambda + \sum_{k=1}^{N_a} \sum_{j=1}^{2} s_j^k T_{qj}^{k^\top} \gamma_j^k \end{bmatrix} \quad (11)$$

Using the R.H.S. equality of (3) in (11), we obtain,

$$\dot{W} = \dot{q}^\top \left(\tau - \Psi_q^\top \Psi_b^{-\top} \gamma_0 + \sum_{k=1}^{N_a} \sum_{j=1}^{2} s_j^k \tilde{T}_{qj}^{k^\top} \gamma_j^k \right) \quad (12)$$

Applying the proposed control law from (8) in (12), we obtain,

$$\dot{W} = - V_b^\top D_0 V_b - \sum_{k=1}^{N_a} \sum_{j=1}^{2} s_j^k V_j^{k^\top} D_{jk} V_j^k$$
$$- \dot{q}^\top (N_0^\top P_0 N_0 + \sum_{k=1}^{N_a} \sum_{j=1}^{2} N_j^{k^\top} P_{jk} N_j^k) \dot{q} \le 0 \quad (13)$$

which proves the uniform stability of the controller error dynamics. Invoking LaSalle's invariance principle, the convergence of the pose errors follows. ∎

Applicability of the controller for different morphologies: The control law defined in Theorem 1 can be applied to the different morphologies shown in Fig. 1 for executing the different operations reported in n Sec. 1 -1. To apply (8), we use the recursive computation of forward kinematics and the Jacobians as shown in Garofalo et al. (2013). To this end, a base-frame needs to be defined for the kinematic chain. In this paper, the base-frame for each arm is chosen to be $\{\mathcal{E}_1^{(\bullet)}\}$, and the state measurements are used to compute the forward kinematics, g_2^k, the base Jacobian $J_b^k = g_2^{k^{-1}} \frac{\partial g_2^k}{\partial g_1^k}$ and the manipulator Jacobian $J_q^k = g_2^{k^{-1}} \frac{\partial g_2^k}{\partial q^k}$. The inverted kinematic chain quantities from $\{\mathcal{E}_2^k\}$ to $\{\mathcal{E}_1^k\}$, are obtained by transforming g_2^k, J_b^k, J_q^k as $g_2^{k^{-1}}, J_b^{k^{-1}}, -J_b^{k^{-1}} J_q^k$, respectively. This approach is exploited for torque command generation in the controller to perform the operations summarized in Sec. 1-1. In the following, two operations are explained as example and the remaining are summarized in table 1.

Morphology 1-arm - operation (i): Here, there is no defined torso frame, and, hence, $\Phi(\eta_0) = 0$ and $\gamma_0 = V_0 = 0_6$. For the walking operation, there are two possible constraints described by (2a) and (2b). For the former, $\Psi_b = \mathbb{I}_{6,6}$, $\Psi_q = 0_{6,n_a}$, $T_{b1} = J_b$ and $T_{q1} = J_q$. For the latter, $\Psi_b = J_b$, $\Psi_q = T_{q2}$, $T_{b2} = \mathbb{I}_{6,6}$ and $T_{q2} = 0_{6,n_a}$. Us-

ing this, from (8), we obtain, $\tau = -J_q^\top \mathrm{PD}_2 + \tau_n$ for the former, and $\tau = J_q^\top J_b^{-\top} \mathrm{PD}_1 + \tau_n$ for the latter. The two control laws above are similar to the fixed-base Jacobian transposed controllers. In particular, J_q and $-J_b^{-1}J_q$ are the manipulator Jacobians in the forward and inverted kinematic chain operation, respectively, while alternating base constraints (2a) and (2b).

Morphology 2-arms - operation (ii): For torso operation, the constraints are defined by (2a) and (2b) corresponding to the arms labelled 1 and 2. In this case, $\Psi_b^\top = \begin{bmatrix} \tilde{J}_b^{1^\top} & \tilde{J}_b^{2^\top} \end{bmatrix}$, where $\tilde{J}_b^k = J_b^k \mathrm{Ad}_{g_{10}^k}$ and Ad_g is the Adjoint operator (Bullo and Murray (1999)) of any pose g. Here, g_{10} accounts for the torso kinematics, i.e., the pose of $\{\mathcal{E}_0\}$ relative $\{\mathcal{E}_1^1\}$. Also, $\Psi_q^\top = \mathrm{blkdiag}(J_q^1, J_q^2)$, and from (8), we obtain, $\tau = -\mathrm{blkdiag}(J_q^1, J_q^2)^\top \Psi_b^{\dagger^\top} \mathrm{PD}_0 + \tau_n$.

Following the same steps, the control law proposed in (8) results to be valid for all the operations defined in Sec. 1-1 and the corresponding quantities with the control laws are reported in Table 1. We conclude that the unified control approach in Theorem 1 is able to handle all the morphologies and operations considered in this paper. A key observation is that all the case-specific control laws depend upon J_b^k, J_q^k for the kth arm. This implies that the CPU of each arm could perform a decentralized computation of its own Jacobians and forward kinematics, which are provided to the CPU of the torso for whole-body centralized control. This might reduce the computational overhead for the torso when additional arms are attached.

4. CO-SIMULATION FRAMEWORK FOR CONTROL PROTOTYPING

For control prototyping, a Co-simulation was developed, in which (1) was simulated by an external dynamics engine, `CoppeliaSim`, formerly known as `V-REP` (Rohmer et al. (2013)), and the control software was developed in `MATLAB/Simulink`. The holonomic constraints in (2) were implemented using the suctionPad functionality in `CoppeliaSim`, which creates an overlap constraint, i.e., the two pertinent objects in close proximity will overlap their respective position/orientation to create dynamics loop closure constraints. Specifically, the suctionPad objects were added on each of the tiles of the breadboard shown in Fig. 1-**D** in a way that reflected the kinematics (not geometry) of the SIs. Thus, in the event that the end-effector of the MAR was in close proximity (below a specified threshold) of the suctionPad object, the former will be constrained to the tile structure. An overview of the developed framework is shown in Fig. 2. As can be seen, the external dynamics engine (`CoppeliaSim`) provides feedback with respect to the state of the plant and the controller possesses recursive kinematics and dynamics computation. Furthermore, the designed Co-simulation
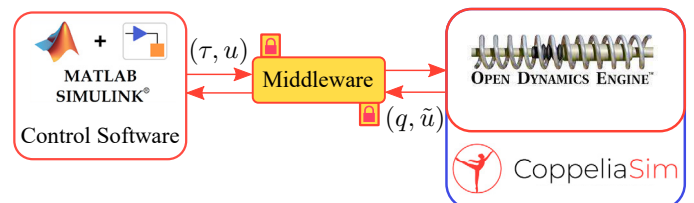

Figure 2. Co-simulation framework for Control Prototyping of the MAR system. Time-step: — 1[ms], — 10[ms]

Morphology	Op.	Constraint	Ψ_b	Ψ_q	s	T_b	T_q	$\tau - \tau_n$
A ($N_a = k = 1$)	$(i),(ii)$	(2a)	$\mathbb{I}_{6,6}$	$0_{6,n_a}$	$\times$	$T_{b1} = J_b$	$T_{q1} = J_q$	$-J_q^\top \mathrm{PD}_2$
	$(i),(ii)$	(2b)	J_b	T_{g2}	$\times$	$T_{b2} = \mathbb{I}_{6,6}$	$T_{q2} = 0_{6,n_a}$	$J_q^\top J_b^{-\top} \mathrm{PD}_1$
B ($N_a = 1$)	$(i),(ii)$	(2b)	$J_b \mathrm{Ad}_{g_{10}} = \tilde{J}_b$	J_q	$s_1^1 = 0, s_2^1 = 1$	$\times$	$\times$	$J_q^\top \tilde{J}_b^{-\top} \mathrm{PD}_0$
	$(i),(ii)$	(2c)	$\mathbb{I}_{6,6}$	$0_{6,n_a}$	$s_1^1 = 0, s_2^1 = 1$	$T_{b2} = \tilde{J}_b$	$T_{q2} = J_q$	$-J_q^\top \mathrm{PD}_2$
C ($N_a = 2$)	(i)	(2b)^1	$J_b^1 \mathrm{Ad}_{g_{10}} = \tilde{J}_b^1$	$\begin{bmatrix} J_q^1 \\ 0_{6,n_a} \end{bmatrix}$	$s_1^{(\bullet)} = 0, s_2^{(\bullet)} = 1$	$T_{b2}^2 = \tilde{J}_b^2 = J_b^2 \mathrm{Ad}_{g_{10}}^2$	$T_{q2}^2 = \begin{bmatrix} 0_{6,n_a} \\ J_q^2 \end{bmatrix}$	$\begin{bmatrix} J_q^{1\top} \tilde{J}_b^{1-\top} \tilde{J}_b^{2-\top} \\ -J_q^{2\top} \end{bmatrix} \mathrm{PD}_2^2$
C ($N_a = 2$)	(i)	(2b)^2	$\tilde{J}_b^2$	$\begin{bmatrix} 0_{6,n_a} \\ J_q^2 \end{bmatrix}$	$s_1^{(\bullet)} = 0, s_2^{(\bullet)} = 1$	$T_{b2}^1 = \tilde{J}_b^1$	$T_{q2}^1 = \begin{bmatrix} J_q^1 \\ 0_{6,n_a} \end{bmatrix}$	$\begin{bmatrix} -J_q^{1\top} \\ J_q^{2\top} \tilde{J}_b^{2-\top} \tilde{J}_b^{1\top} \end{bmatrix} \mathrm{PD}_2^1$
C ($N_a = 2$)	(ii)	(2b)^1, (2b)^2	$\Psi_b^\top = \begin{bmatrix} \tilde{J}_b^{1\top} & \tilde{J}_b^{2\top} \end{bmatrix}$	$\Psi_q = \mathrm{blkdiag}(J_q^1, J_q^2)$	$s_1^{(\bullet)} = 0, s_2^{(\bullet)} = 1$	$\times$	$\times$	$\mathrm{blkdiag}(J_q^1, J_q^2)^\top \Psi_b^\dagger \mathrm{PD}_0$
C ($N_a = 2$)	(iii)	(2c)	$\mathbb{I}_{6,6}$	$0_{6,n_a}$	$s_1^{(\bullet)} = 0, s_2^{(\bullet)} = 1$	$T_{b2}^1 = J_q^1, T_{b2}^1 = J_q^2$	$T_{q2}^1 = \begin{bmatrix} J_q^1 \\ 0_{6,n_a} \end{bmatrix}, T_{q2}^2 = \begin{bmatrix} 0_{6,n_a} \\ J_q^2 \end{bmatrix}$	$\begin{bmatrix} J_q^{1\top} \mathrm{PD}_2^1 \\ J_q^{2\top} \mathrm{PD}_2^2 \end{bmatrix}$

Table 1. A Unified controller to perform in-orbit operations with a reconfigurable Multi-Arm Robot. The superscripts and subscripts denote the labels for the arm and the end-effector, respectively, ($\bullet$) applies to all the arms and $\times$ indicates that the quantities are not required.

offers the possibility to control the joints directly at 1kHz. The developed Co-simulation framework will be used for validation of advanced operations.

5. CO-SIMULATION RESULTS

The Co-simulation framework presented in Sec. 4 is utilized to validate the developed unified controller in Sec. 3. Results will be presented for three scenarios, which are the most representative, namely the walking with 1-arm , the control of torso and the walking for the 2-arm system. In the following the orientation error is represented by $\Delta R = \mathrm{sk}(\breve{\eta}_j^{\;k})^\vee . \frac{180}{\pi}$.

A Morphology 1-arm - (i): Walking operation.
Fig. 3 shows the end-effector error in position and orientation during the motion of the 1-arm along three tiles. At t=0, the arm has an error in position and orientation that converges to zero at t = 27s, consequentially the SI is engaged to lock the end-effector to the first tile. A new pose is given as input to the controller at t=27.1s to reach the second tile, which occurs at t=50s. The same operation is repeated at t=50.1s. The increase in error, at t=27.1s (t=50s), marks a new step, i.e. a new desired pose is set for the unconstrained end-effector. The corresponding joint torque commanded by the controller during the walking operation are shown in Fig. 4.
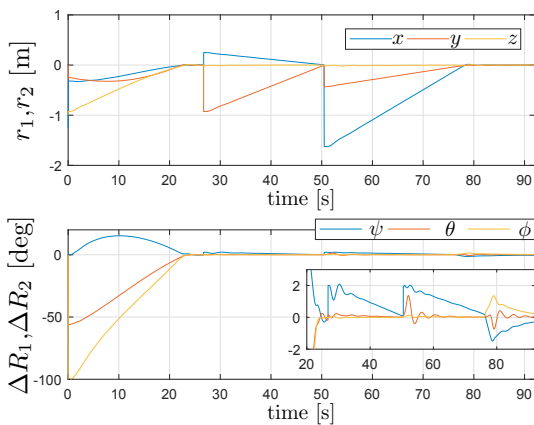
C Morphology 2-arms - (ii): Torso operation.
The designed controller is applied to perform the torso operation, i.e., moving the torso towards a tile while the two arms are constrained. Fig. 5 shows the position and
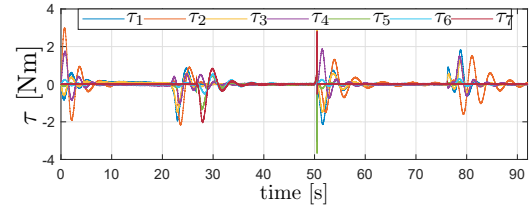

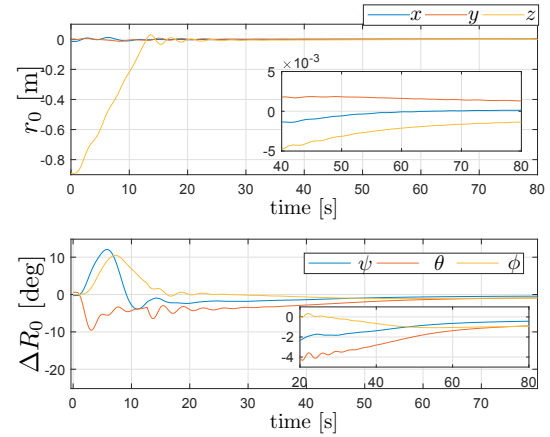Figure 4. A Morphology 1-arm - commanded joint torques.

Figure 5. C Morphology 2-arms - (ii): error in position (top) and orientation (bottom) during the torso operation.

orientation error during this operation the steady-state error is below 2 mm and 1 deg. The corresponding torques commanded to the arm 1 and arm 2 (which are latched to the SIs) are shown in Fig. 6, respectively.

C Morphology 2-arms - (i): Walking operation.
The walking operation for the dual arm system with torso considers a motion towards 5 different tiles. A snapshot of the walking procedure is shown in Fig. 7, where the system moves from its initial position at t=0 to the first tile with the arm 1. At t =39s, the SI is engaged and later the second arm can move towards the second tile (t=50s) and performing a second latch with the SI at t = 60s. The walking operation continues for 110s and the engagement and disengagement of the SIs is shown in Fig. 8, where the state 1 indicates the engage of the SI and 0 the disengage. The error in position and orientation during this walking operation is shown in Fig. 9.
The results show the effectiveness of the developed unified controller in performing several operations with different morphologies of the MAR system.

Figure 3. A Morphology 1-arm - (i): error in position (top) and orientation (bottom) during the walking operation.
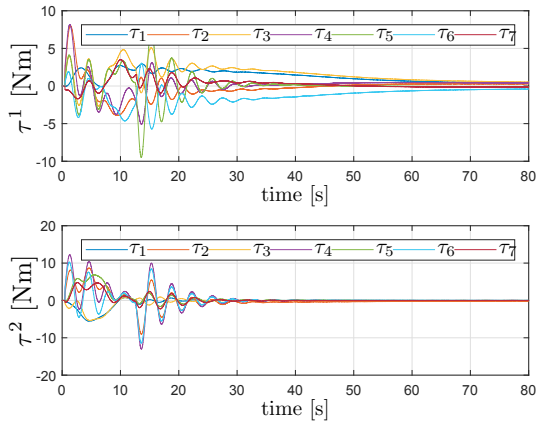
Figure 6. C Morphology 2-arms - (ii) commanded joint torques (top) of arm 1 and arm 2 (bottom).
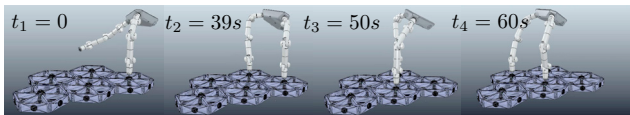

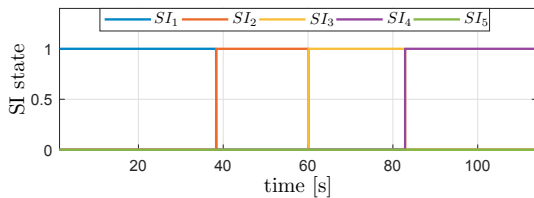Figure 7. C Morphology 2-arms - (i): snapshots of walking operation.

Figure 8. C Morphology 2-arms - (i): engage and disengage of SI during the walking operation.
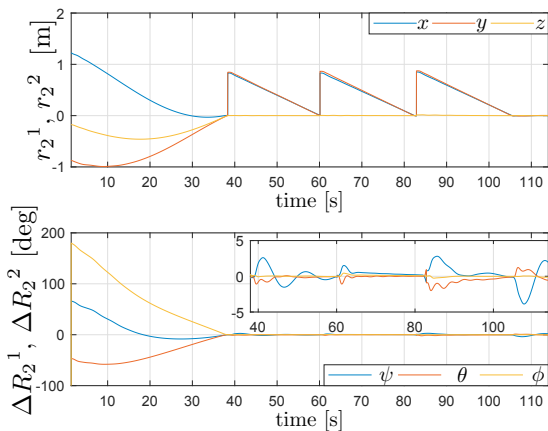

Figure 9. C Morphology 2-arms - (i): error in position and orientation.

6. CONCLUSION

In this paper, a unified controller has been designed for a reconfigurable robotic system composed of a torso and independent arms. This passivity-based controller is compliant against external contacts, e.g. latching with the SIs. The validation results for the MIRROR case proved the effectiveness of the controller for the different morphologies of the MAR system and operations, such as walking with 1-arm or 2-arms through dedicated interface of a space telescope. It is worth mentioning that the controller not only accommodates independent control of each arm in a decentralized manner as shown, e.g. for the case A.(i) and A.(ii), but also a centralized control to provide redundancy to the whole-body system.

ACKNOWLEDGEMENTS

REFERENCES

Belvin, W.K. et al. (2016). In-space structural assembly: Applications and technology. In *3rd AIAA Spacecraft Structures Conf.*

Bullo, F. and Murray, R. (1999). Tracking for fully actuated mechanical systems: a geometric framework. *Automatica*, 35(1), 17–34.

De Sapio, V. (2011). Task-level control of motion and constraint forces in holonomically constrained robotic systems. *IFAC Proceedings Volumes*, 44(1), 14622–14629. 18th IFAC World Congress.

Deremetz, M. et al. (2020). Mosar-wm: A relocatable robotic arm demonstrator for future on-orbit applications. In *71st International Astronautical Congress (IAC) – The CyberSpace Edition.*

Deremetz, M. et al. (2021). Concept of operations and preliminary design of a modular multi-arm robot using standard interconnects for on-orbit large assembly. In *72st International Astronautical Congress (IAC)*.

Dietrich, A. et al. (2021). Practical consequences of inertia shaping for interaction and tracking in robot control. *Control Engineering Practice*, 114, 104875.

Garofalo, G. et al. (2013). On the closed form computation of the dynamic matrices and their differentiations. In *IEEE/RSJ International Conference on Intelligent Robots and Systems (IROS)*, 2364–2359.

Henze, B. et al. (2016). Passivity-based whole-body balancing for torque-controlled humanoid robots in multi-contact scenarios. *The International Journal of Robotics Research*, 35(12), 1522–1543.

Kajita, S. (2019). *Linear Inverted Pendulum-Based Gait*, 905–922. Springer Netherlands, Dordrecht.

Lee, N.N. et al. (2016). Architecture for in-space robotic assembly of a modular space telescope. *Journal of Astronomical Telescopes, Instruments, and Systems*, 2(4), 041207.

Letier, P. et al. (2020). Hotdock: Design and validation of a new generation of standard robotic interface for on-orbit servicing. In *71st International Astronautical Congress (IAC) – The CyberSpace Edition.*

Mishra, H. et al. (2020). A geometric controller for fully-actuated robotic capture of a tumbling target. In *American Control Conference (ACC)*, 2150–2157.

Popovic, M.B. et al. (2005). Ground reference points in legged locomotion: Definitions, biological trajectories and control implications. *The International Journal of Robotics Research*, 24(12), 1013–1032.

Righetti, L. et al. (2013). Optimal distribution of contact forces with inverse-dynamics control. *The International Journal of Robotics Research*, 32(3), 280–298.

Roa, M.A. et al. (2017). Robotic technologies for in-space assembly operations. In *Symposium on Advanced Space Technologies in Robotics and Automation (ASTRA)*.

Roa, M.A. et al. (2019). In-space robotic assembly of large telescopes. In *Symposium on Advanced Space Technologies in Robotics and Automation (ASTRA)*.

Rohmer, E. et al. (2013). V-REP: A versatile and scalable robot simulation framework. In *2013 IEEE/RSJ International Conference on Intelligent Robots and Systems*, 1321–1326.

Saccon, A. et al. (2017). On centroidal dynamics and integrability of average angular velocity. *IEEE Robotics and Automation Letters*, 2(2), 943–950.

Vukobratovic, M. and Borovac, B. (2004). Zero-moment point — thirty five years of its life. *International Journal of Humanoid Robotics*, 01(01), 157–173.